Ultrasound in Med. & Biol., Vol. 43, No. 11, pp. 2651–2669, 2017

0301-5629

http://dx.doi.org/10.1016/j.ultrasmedbio.2017.06.029

● *Original Contribution*

ULTRASOUND IMPROVES THE DELIVERY AND THERAPEUTIC EFFECT OF NANOPARTICLE-STABILIZED MICROBUBBLES IN BREAST CANCER XENOGRAFTS

Sofie Snipstad,* Sigrid Berg,[†‡] Ýrr Mørch,[§] Astrid Bjørkøy,* Einar Sulheim,*[§] Rune Hansen,[†‡] Ingeborg Grimstad,* Annemieke van Wamel,* Astri F. Maaland,* Sverre H. Torp,[¶‖] and Catharina de Lange Davies*

*Department of Physics, Norwegian University of Science and Technology, Trondheim, Norway; [†]SINTEF Technology and Society, Trondheim, Norway; [‡]Department of Circulation and Medical Imaging, Norwegian University of Science and Technology, Trondheim, Norway; [§]SINTEF Materials and Chemistry, Trondheim, Norway; [¶]Department of Laboratory Medicine, Children's and Women's Health, Norwegian University of Science and Technology, Trondheim, Norway; and [‖]Department of Pathology, St. Olav's University Hospital, Trondheim, Norway

(*Received* 16 *March* 2017; *revised* 16 *June* 2017; *in final form* 29 *June* 2017)

Abstract—Compared with conventional chemotherapy, encapsulation of drugs in nanoparticles can improve efficacy and reduce toxicity. However, delivery of nanoparticles is often insufficient and heterogeneous because of various biological barriers and uneven tumor perfusion. We investigated a unique multifunctional drug delivery system consisting of microbubbles stabilized by polymeric nanoparticles (NPMBs), enabling ultrasound-mediated drug delivery. The aim was to examine mechanisms of ultrasound-mediated delivery and to determine if increased tumor uptake had a therapeutic benefit. Cellular uptake and toxicity, circulation and biodistribution were characterized. After intravenous injection of NPMBs into mice, tumors were treated with ultrasound of various pressures and pulse lengths, and distribution of nanoparticles was imaged on tumor sections. No effects of low pressures were observed, whereas complete bubble destruction at higher pressures improved tumor uptake 2.3 times, without tissue damage. An enhanced therapeutic effect was illustrated in a promising proof-of-concept study, in which all tumors exhibited regression into complete remission. (E-mail: sofie.snipstad@ntnu.no) **© 2017 The Authors. Published by Elsevier Inc. on behalf of World Federation for Ultrasound in Medicine & Biology. This is an open access article under the CC BY-NC-ND license (http://creativecommons.org/licenses/by-nc-nd/4.0/).**

Key Words: **Drug delivery, Focused ultrasound, Microbubbles, Nanomedicine, Poly(alkyl cyanoacrylate), Cabazitaxel, Triple-negative breast cancer.**

INTRODUCTION

Normally in chemotherapy, only a small fraction of the injected dose, 0.001% to 0.01% (Gerber et al. 2009; Kurdziel et al. 2011), reaches the tumor in patients. Most of the dose accumulates in healthy tissue, causing severe side effects, or is rapidly excreted. Nanoparticles (NPs) have attracted great attention in drug delivery and diagnostics (Lammers et al. 2010), especially in cancer. Leaky tumor vasculature (Hanahan and Weinberg 2011) and non-functional lymphatics result in the enhanced permeability and retention (EPR) effect, which allows NPs to selectively extravasate and accumulate in tumors, while the healthy tissue is less exposed (Maeda et al. 2000). Compared with conventional chemotherapy, incorporation of drugs into NPs can therefore potentially improve pharmacokinetics, increase efficacy and reduce toxicity of the drug, resulting in reduced dose-limiting side effects. Furthermore, potent drugs with poor solubility or high toxicity, which are a hurdle for the pharmaceutical industry (Desai 2012), can benefit from encapsulation.

Promising pre-clinical therapeutic studies have resulted in the development of several nanomedicine formulations that are being tested in clinical trials (Etheridge et al. 2013; He et al. 2015; Taurin et al. 2012). Many nanomedicines have exhibited reduced side effects (He et al. 2015), but limited efficacy in clinical trials (Wilhelm et al. 2016), and the progression of

Address correspondence to: Sofie Snipstad, Department of Physics, Norwegian University of Science and Technology (NTNU), Høgskoleringen 5 Trondheim 7491, Norway. E-mail: sofie.snipstad@ntnu.no

Conflict of interest disclosure: The authors declare no conflict of interest.

anti-cancer nanomedicines into the clinic has been slow. To date, only a few are used clinically. For successful delivery, the NPs must circulate in the blood for a sufficient time, extravasate from the vasculature, penetrate the extracellular matrix (ECM) and deliver their payload to the intracellular targets. However, there are numerous barriers that limit therapeutic response (Anchordoquy et al. 2017; Desai 2012), such as the heterogeneous EPR effect between and within tumors (Hansen et al. 2015; He et al. 2015; Maeda 2015; Prabhakar et al. 2013), poor vascularization, high interstitial fluid pressure, high tumor cell density (Padera et al. 2004) and dense ECM (Chauhan et al. 2011; Desai 2012). A recently published meta-analysis including 117 reports found that a median of only 0.7% of the injected dose reached the tumor (Wilhelm et al. 2016). This emphasizes the need for new strategies that can increase controlled delivery to the target.

Focused ultrasound (FUS), particularly when combined with microbubbles (MBs), has emerged as a promising method by which the delivery of drugs or NPs to tumor tissue can be improved in a non-invasive manner (Burke et al. 2014; Frenkel 2008; Graham et al. 2014; Heath et al. 2012; Lammertink et al. 2015; Pitt et al. 2004; van Wamel et al. 2016), and has recently been reported to increase survival in mice (Burke et al. 2014; Kotopoulis et al. 2014; van Wamel et al. 2016) and humans with inoperable pancreatic cancer (Dimcevski et al. 2016). FUS treatment is non-invasive, and can be applied locally for various forms of tumors. Another important application of low-intensity FUS in conjunction with intra-venously administered MBs is the transient and selective opening of the blood–brain barrier, as reported in small animals (Burgess et al. 2011; Hynynen et al. 2001) and non-human primates (Downs et al. 2015; Marquet et al. 2011). This opens the possibility of treating aggressive glioblastoma and other diseases in the central nervous system. Currently, there are two ongoing clinical trials in glioblastoma patients (ClinicalTrials.gov Identifier NCT02343991 and NCT02253212) (Carpentier et al. 2016).

Focused ultrasound for therapeutic purposes can be employed to create thermal and mechanical effects such as cavitation and radiation force (Frenkel 2008; Pitt et al. 2004). Cavitation is the creation and oscillation of gas bubbles on exposure to an acoustic wave. At relatively low pressures, acoustic pressure waves will cause the stable cavitation of MBs. Stable cavitation is characterized by sustained bubble radius oscillation about its equilibrium. This generates microstreaming, fluid flow around the MBs (Elder 1959). Resulting shear stresses on the blood vessel wall when the MBs are close to or in contact with the endothelium can cause the formation of small pores and thus increase vascular permeability and can enhance endocytosis (Afadzi et al. 2013; Lentacker et al. 2014; Meijering et al. 2009). At higher pressures, the oscillations will increase in amplitude, become more transient and result in a violent collapse of the bubbles. This is termed *inertial cavitation* and can lead to the formation of shock waves and jet streams in the vasculature, which can create both temporary and permanent pores in the capillary wall and in cell membranes (Lentacker et al. 2014). The probability of inertial cavitation in a medium is determined by the mechanical index (MI), which is given by the peak negative pressure of the ultrasound (US) wave divided by the square root of its center frequency. It is reasonable to assume that the probability of occurrence of permanent tissue damage increases above the threshold for inertial cavitation. FUS can thus locally increase extravasation across the capillary wall and potentially improve penetration through the ECM, thereby improving the accumulation and distribution of NPs and drugs in tumors (Burke et al. 2014; Dimcevski et al. 2016; Frenkel 2008; Kotopoulis et al. 2014; Lin et al. 2010, 2012; van Wamel et al. 2016; Wang et al. 2015).

A unique multifunctional drug delivery system consisting of MBs stabilized by polymeric NPs (NPMBs) to be used in image-guided and FUS-mediated drug delivery, as illustrated in Figure 1, has been developed (Mørch et al. 2015). Biodegradable poly(alkyl cyanoacrylate) (PACA) NPs (Nicolas and Couvreur 2009; Vauthier et al. 2003, 2007) are prepared in a one-step synthesis, can encapsulate a range of drugs or contrast agents with high loading capacity and can be functionalized with polyethylene glycol (PEG) (Mørch et al. 2015). One type of PACA NPs has already reached phase III clinical trials for treatment of liver cancer (Livatag, Onxeo, Opole Voivodeship, Poland; ClinicalTrials.gov Identifier NCT01655693) (Soma et al.

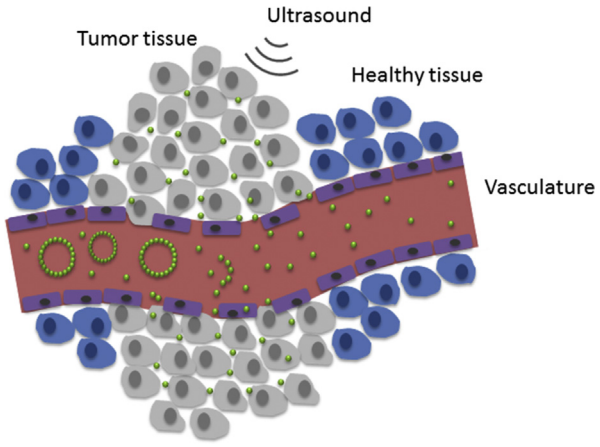

Fig. 1. Schematic of enhanced drug delivery to tumor tissue by use of focused ultrasound and nanoparticle-stabilized microbubbles (in *green*).

2012). The MBs are formed by self-assembly of NPs into a shell. We previously reported that this platform, in combination with FUS, can be employed to improve delivery of NPs to xenograft tumors in mice (Eggen et al. 2014) and delivery across the blood–brain barrier in healthy rats (Åslund et al. 2015). In our previous work, poly(butyl cyanoacrylate) (PBCA) NPs were used, whereas poly(2-ethyl-butyl cyanoacrylate) (PEBCA) NPs were applied in the present study. Because of a longer and branched alkyl monomer chain, PEBCA NPs probably have a slower degradation rate (Muller et al. 1992; Sulheim et al. 2016), which might be therapeutically favorable.

In the present work, the PEBCA NPs were characterized with respect to *in vitro* cellular uptake and efficacy in a triple-negative breast cancer cell line. *In vivo* circulation half-life and biodistribution of NPs were determined, and circulation of the MBs was evaluated. The main aim of the present study was to systematically study the effect of various US parameters, and investigate the mechanisms of US-mediated delivery, to determine the importance of cavitation and bubble destruction for improved extravasation and enhanced NP delivery to tumor tissue. Furthermore, we aimed to determine tolerable acoustic pressures that enhance delivery of the nanomedicine to tumor tissue, and to determine if the increased delivery had a therapeutic benefit. Subcutaneous human breast cancer xenografts were grown in athymic mice, and NPMBs were injected intra-venously, whereas the tumors were treated with FUS of various pressures and burst lengths. The delivery of NPs to tumors was evaluated by confocal microscopy on frozen tumor sections. To evaluate whether the increased delivery had a therapeutic benefit, the first proof-of-concept pre-clinical treatment study was performed with NPMBs encapsulating the anti-cancer drug cabazitaxel.

METHODS

Synthesis and characterization of nanoparticles and microbubbles

PEGylated PEBCA NPs were synthesized by mini-emulsion polymerization as described previously (Mørch et al. 2015). Briefly, an oil phase consisting of 2-ethyl-butyl cyanoacrylate (monomer, Henkel Loctite, Düsseldorf, Germany) containing 0.1 wt% methane sulfonic acid (Sigma-Aldrich, St. Louis, MO, USA), 2 wt % Miglyol 812 (co-stabilizer, Cremer, Cincinnati, OH, USA) and 0.8 wt% azo bis-dimethyl valeronitrile (V65, oil-soluble radical initiator, Waco, Osaka, Japan) was prepared. Fluorescent particles for optical imaging were prepared by adding either NR668 (modified NileRed [Klymchenko et al. 2012], custom synthesis, 0.5 wt%) or IR-780 Lipid (near-infrared dye, custom synthesis, CEA, Grenoble, France, 0.5 wt%) to the oil phase. Particles containing cytostatic drug for treatment were prepared by adding cabazitaxel (10 wt%, Biochempartner, Wuhan, Hubei, China) to the oil phase.

An aqueous phase consisting of 0.1 M HCl containing Brij L23 (10 mM, 23 PEG units, MW 1225, Sigma-Aldrich) and Kolliphor HS15 (10 mM, 15 PEG units, MW 960, Sigma-Aldrich) was added to the oil phase and immediately sonicated for 3 min on ice (6 × 30-s intervals, 60% amplitude, Branson Ultrasonics digital sonifier 450, Danbury, CT, USA). The solution was kept on magnetic stirring for 1 h at room temperature before adjusting the pH to 5 using 0.1 M NaOH. The polymerization was continued for 2 h at room temperature before increasing the temperature to 50°C for 8 h while the solution was rotated (15 rpm). The dispersion was dialyzed (Spectra/Por dialysis membrane MWCO 100,000 Da, Spectrum Labs, Rancho Dominguez, CA, USA) against 1 mM HCl to remove unreacted PEG. The dialysate was replaced three times. Details regarding PEGylation of the NP-platform have been published previously (Åslund et al. 2017; Baghirov et al. 2017; Mørch et al. 2015). The size, polydispersity index (PDI) and ζ potential of the NPs were measured by dynamic light scattering using a Zetasizer Nano ZS (Malvern Instruments, Malvern, UK). To calculate the amount of encapsulated drug, the drug was extracted from the particles by dissolving them in acetone (1:10) and quantified by liquid chromatography coupled to mass spectrometry (LC-MS/MS, Agilent 6490 triple quadrupole coupled with Agilent 1290 HPLC, Agilent Technologies, Santa Clara, CA, USA).

The NPMBs were prepared by self-assembly of the NPs (1 wt%, 10 mg/mL) at the gas–water interface by the addition of 0.5% casein in phosphate-buffered saline and vigorous stirring using an Ultra-Turrax (T-25, IKA-Werke, Staufen, Germany), as described (Mørch et al. 2015). Perfluoropropane (F2 Chemicals, Preston, Lancashire, UK) was used instead of air for increased circulation time. The average MB diameter, size distribution and concentration were determined using light microscopy and image analysis (ImageJ 1.48 v, National Institutes of Health, Bethesda, MA, USA). The NPMB solution is a combination of free NPs and NPMBs, where only a small percentage of the NPs are located on MBs. The MBs were characterized with respect to acoustic destruction as described below.

Cell culture

Triple-negative human breast adenocarcinoma cells (MDA-MB-231, kind gift from the Department of Circulation and Medical Imaging, NTNU, Trondheim, Norway, purchased from HTB-26, American Type Culture Collection, Manassas, VA, USA) were cultured in Roswell Park Memorial Institute (RPMI) 1640 medium (21875-034, Gibco, Thermo Fisher Scientific, Waltham,

MA, USA), supplemented with 10% fetal bovine serum (Sigma-Aldrich). The cells were kept at 37°C and 5% CO_2 and maintained in exponential growth. The antibiotic gentamicin (0.1%, Sigma-Aldrich) was added to the medium for cells that were to be implanted *in vivo* and for *in vitro* toxicity studies.

Animals and tumors

All experimental procedures were approved by the Norwegian Animal Research Authorities. Female Balb/c nude mice (Envigo, Cambridgeshire, UK) were purchased at 7–8 wk of age, 16–21 g. They were housed in specific pathogen-free conditions, in groups of four or five in individually ventilated cages (Model 1284 L, Tecniplast, Lyon, France) at temperatures of 22°C–23°C, 50%–60% relative humidity, 70 air changes per hour, with *ad libitum* access to food and sterile water.

Subcutaneous xenograft tumors were grown from breast cancer MDA-MB-231 cells. Animals were anesthetized by inhalation of 2%–3% isoflurane in O_2 and NO_2 (Baxter, Deerfield, IL, USA), before 50 μL medium containing 3×10^6 cells was slowly injected subcutaneously into the lateral aspect of the left hind leg, between the knee and the hip. Over the next weeks, the animals were weighed and the tumors measured using calipers two to three times per week. Tumor volume was calculated as $\pi lw^2/6$, where l and w are the length and width of the tumor, respectively. Tumor growth did not affect the weight of the animals.

During experiments, the animals were anesthetized by a subcutaneous injection of fentanyl (0.05 mg/kg, Actavis Group HF, Hafnarfirdi, Iceland), medetomidine (0.5 mg/kg, Orion Pharma, Oslo, Norway), midazolam (5 mg/kg, Accord Healthcare Limited, North Harrow, United Kingdom) and water (2:1:2:5) at a dose of 0.1 mL per 10 g. When necessary, a subcutaneous injection of atipemazol (2.5 mg/kg, Orion Pharma, Oslo, Norway), flumazenil (0.5 mg/kg, Fresenius Kabi, Bad Homburg vor der Höhe, Germany) and water (1:1:8) at a dose of 0.1 mL per 10 g was used as antidote to terminate the anesthesia. During all experiments, the body temperature of the animals was maintained by external heating, and eyes were kept moist with Viscotears Liquid gel (Alcon, Fort Worth, TX, USA). At the end of the experiment, anesthetized animals were euthanized by cervical dislocation.

In vivo *circulation half-life of nanoparticles*

The mice were anesthetized as described above, and NPs containing NR668 were diluted to 7 mg/mL in phosphate buffer and injected intra-venously as a bolus of 200 μL through the lateral tail vein in five mice (70 mg/kg). Blood samples of 10–15 μL were drawn from the saphenous vein pre-injection and 10 min, 30 min, and 1, 2, 4, 6 and 24 h post-injection. Between the 4-, 6- and 24-h samples, the animals were placed in a recovery rack (Blue Line, Scanbur, Copenhagen, Denmark) where the temperature was kept at 28°C to avoid hypothermia. Blood samples were diluted in 40 μL 10 IU/mL heparin (Leo Pharma A/S, Ballerup, Denmark) and vortexed (444-1372, VWR, Radnor, PA, USA), before they were centrifuged at 3000 rpm for 7 min (Micromax, International Equipment Company [IEC], Needham, MA, USA) Fluorescence in the supernatant was measured with a spectrophotometer (Infinite 200 Pro, Tecan, Männedorf, Switzerland) by excitation at 535 nm (bandwidth 9 nm) and detection at 620 nm (bandwidth 20 nm). A 384-well plate (Corning, Corning, NY, USA) with 10 μL from each blood sample was analyzed. Fluorescence intensity per volume of blood diluted in heparin, plotted as a function of time, was fitted by a mono-exponential decay curve ($f(t) = ae^{-bt}$) using SigmaPlot (12.0, Systat Software, San Jose, CA, USA), resulting in a circulation half-life ($t_{1/2} = \ln(2)/b$).

In vivo *circulation of microbubbles*

Inflow and circulation of fluorescently labeled NPMBs in tumors were imaged with contrast-enhanced US using a Vevo 2100 and the MS250 probe (FujiFilm VisualSonics, Toronto, ON, Canada). The tail veins of anesthetized mice were cannulated (BD Neoflon 24 G, Becton Dickinson & Company, Franklin Lakes, NJ, USA), and 200 μL of NPMBs (10 mg/mL NPs) was injected intra-venously. Perfusion of the tumor was imaged using non-linear contrast-enhanced imaging mode, with a transmit frequency of 18 MHz, a power of 10% and a frame rate of 10 fps. Data were exported using VisualSonics software (1.6.0, FujiFilm VisualSonics, Toronto, ON, Canada) and displayed using MATLAB (R2014 b, The MathWorks, Natick, MA, USA). NPMBs loaded with cabazitaxel were also imaged *in vivo* to ensure that the drug did not affect the circulation, and the inflow and circulation in a kidney were imaged using the same settings and a frame rate of 20 fps.

Biodistribution of nanoparticles

Mice were anesthetized and the lateral tail veins were cannulated as described, before a bolus of 200 μL NPMBs (10 mg/mL NPs, resulting in 100 mg/kg) containing the infrared dye IR-780 lipid was injected. Antidote was administered, and the animals were kept in a recovery rack. Six hours post-injection, animals were euthanized, and the spleen, liver, kidney, heart, lungs, brain and tumor were excised. Organs were imaged using a near infrared Pearl Impulse small animal imaging system (LI-COR Biosciences, Lincoln, NE, USA). Excitation/emission settings were 785 nm/820 nm. Images were processed using ImageJ to quantify the accumulation of NPs. Regions of interest (ROIs) were drawn

around each organ, and the sum of the intensity values of the pixels in the selection was calculated. Nine known concentrations of NPs in phosphate buffer ranging from 0 to 2 mg/mL were imaged to obtain a standard curve (Supplementary Fig. S1, online only, available at http://dx.doi.org/10.1016/j.ultrasmedbio.2017.06.029). From this, the accumulated dose of NPs, as a percentage of the total injected dose and as weight of NPs per weight of tissue, was determined.

Cellular uptake of nanoparticles

In vitro cellular uptake was determined using flow cytometry (FCM) and confocal laser scanning microscopy (CLSM). For quantification with FCM, 300,000 cells in 3 mL medium were seeded in six-well plates (Corning Costar, Sigma-Aldrich), and 30,000 cells in 300 μL medium were seeded in eight-well slides (Ibidi, Martinsried, Germany) for CLSM. Forty-eight hours later, the medium was changed, and at 72 h, the medium was replaced with medium containing 20 μg/mL NPs with NR668. After 3 h incubation, the cells were rinsed two or three times with phosphate-buffered saline (PBS). The cells for FCM were trypsinized (Sigma-Aldrich) and placed on ice until FCM analysis. Incubation was at 37°C, but also at 4°C to ensure that no leakage of the dye was observed (Snipstad et al. 2014, 2016; Sulheim et al. 2016). At this temperature, NP uptake by endocytosis is not expected, and staining of the cells would likely be caused by leakage of the dye.

In FCM (Gallios, Beckman Coulter, Indianapolis, IN, USA), a 561-nm laser was used to excite NR668, and fluorescence was detected at 620 nm using a 30-nm bandpass filter. Cellular fragments, debris and aggregates were excluded from the analysis by gating the side-scatter versus forward-scatter dotplot. Approximately 10,000 events were counted from each sample. The percentage of cells taking up NPs and their median fluorescence intensity were determined using Kaluza Flow Cytometry Analysis software, Version 1.3 (Beckman Coulter).

Confocal laser scanning microscopy imaging (TCS SP8, Leica, Wetzlar, Germany) was performed using a 63 × 1.2 water objective and a pinhole of 1 airy unit. A white light laser at 540 nm was used to excite NR668, and fluorescence was detected at 569–699 nm. The fluorescence signal was superimposed on a bright-field image from the same laser. Images were captured using a frame size of 1024 × 1024 pixels, with a pixel size of 180 nm.

In vitro *toxicity*

Cellular toxicity was studied using the colorimetric AlamarBlue assay (Thermo Fischer Scientific). Cells were seeded in black 96-well plates (Corning, Corning, NY, USA), 2500 cells per 200 μL medium. At 72 h, medium with NPs containing cabazitaxel was added. Concentrations of NPs ranging from 0 to 10,000 ng/mL were used, corresponding to cabazitaxel concentrations of 0 to 1000 ng/mL (10%). Free drug (in polysorbate 80 [Sigma-Aldrich] and ethanol) at the same concentrations, as well as NPs without the drug, were used for comparison. The cells were incubated at 37°C with 5% CO_2 for 24 h, before being rinsed three times with medium. AlamarBlue was diluted 1:10 with medium, and 110 μL was added to each well. Medium with AlamarBlue without cells was used as a blank. The cells were incubated for 2 h at 37°C, protected from light. Fluorescence was measured using a microplate reader (SpectraMax i3 x, Molecular Devices, Sunnyvale, CA, USA), with an excitation wavelength of 550 ± 9 nm and emission detected at 590 ± 20 nm. Metabolically active cells reduced resazurin to the fluorescent resorufin, from which the percentage of viable cells was estimated. Dose–response curves, $f(x) = y_{min} + ((y_{max}–y_{min})/(1 + (x/IC_{50})^k))$, were fitted to the experimental data points using SigmaPlot (four-parameter logistic curve). y_{min} and y_{max} are the minimum and maximum survival values, IC_{50} is the concentration that gives a response halfway between baseline and maximum and k is the slope of the curve. y_{min} and y_{max} were constrained to be between 0 and 100%.

Ultrasound setup

A custom made, single-element focused transducer with a center frequency of 1 MHz (Imasonic, Besancon, France) was used. The signal was generated by a waveform generator (33500 B, Agilent Technologies) and amplified by a 50-dB power amplifier (2100 L, E&I, Rochester, NY, USA). The transducer was mounted at the bottom of a water chamber (Fig. 2a), and a lid with an absorber was placed at the water surface. The animals were placed on the lid, and the tumor-bearing leg was lowered into the water through a 10-mm opening. The tumor was placed in the far field of the FUS beam at a distance of 190 mm, to cover the entire tumor. The water in the tank was heated to 34°C (Trixie aqua pro heater, Zoopermarked, Højbjerg, Denmark) to avoid hypothermia and altered blood flow in the mouse leg (Hyvelin et al. 2013). The transducer had a diameter of 50 mm and a focal distance of 125 mm. It was characterized in a water tank using a hydrophone (HGL-0200, Onda); the beam profile can be found in Supplementary Figure S2 (online only, available at http://dx.doi.org/10.1016/j.ultrasmedbio.2017.06.029). The lateral 3- and 6-dB beam widths at 190 mm had diameters of 6 and 10 mm, respectively. In the axial direction, a 3-dB reduction in pressure was measured at 210 mm.

Characterization of microbubble destruction

Destruction of the NPMBs was evaluated by imaging NPMBs in a flow tube through a water container, where the flow was driven by a peristaltic pump. After

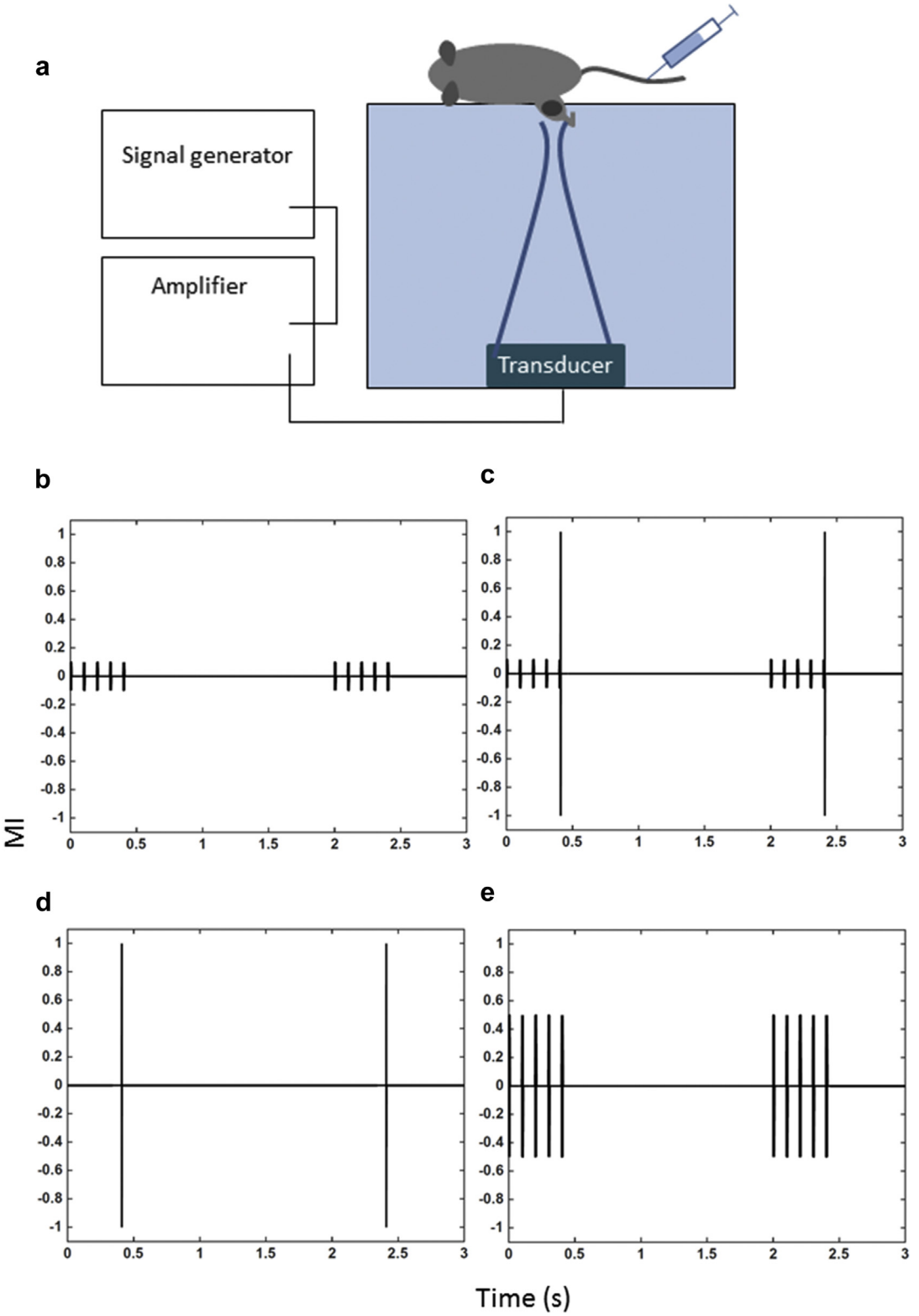

Fig. 2. (a) Schematic of ultrasound setup. The transducer had a diameter of 50 mm and a focal length of 125 mm. Treatment was done in the far field, at 190 mm, where the lateral 3- and 6-dB beam widths were 6 and 10 mm, respectively. (b–e) Schematics of selected ultrasound treatments for (b) group 2, (c) group 3, (d) group 4 and (e) group 6, in which mechanical index (MI) is plotted as a function of time for the first 3 s of each treatment. Each vertical line illustrates a burst.

the flow was stopped, the NPMBs were sonicated by a single burst of 10,000 cycles at MIs of 0.1, 0.25, 0.5 and 1 using the 1-MHz transducer (Imasonic). Simultaneously, the sonicated region of the tube was imaged using an MI of 0.1 at 4 MHz with a clinical US scanner in contrast mode (Vivid E95 scanner and 9 L transducer, GE Healthcare, Chicago, IL, USA). Destruction of MBs was determined by visual inspection.

Ultrasound exposure optimization

To investigate how various acoustical settings in combination with our MBs affected NP accumulation in tumor tissue, subcutaneous tumors in 18 mice were allowed to grow for 4–8 wk until they reached a diameter of approximately 7–8 mm in the longest direction and a volume of approximately 120–250 mm^3. The animals were anesthetized, and the lateral tail veins were cannulated, and NPMBs containing NR668 were injected intra-venously at a dose of 200 μL with 10 mg/mL NPs (100 mg/kg). The US treatment was initialized when the injection started. The mice were randomly distributed to different groups, and tumors were treated with one of six different FUS treatments (Fig. 2). Acoustic pressures ranged from 0.1 to 1 MPa (MIs ranging from 0.1 to 1). All tumors (except group 4) received bursts of 10,000 cycles (10 ms) every 100 ms (local pulse repetition frequency [PRF] = 10 Hz) for a 0.5-s treatment, followed by a 1.5-s break (global PRF = 0.5 Hz, total duty cycle = 2.5%). In the groups in which MB destruction is expected, reperfusion of MBs in the sonicated area is important to allow new MBs to reach the tumor, and thus a PRF of 0.5 Hz was used. For the highest pressure, a short flash of 3 cycles was also investigated. The total treatment time was 2 min. An overview of the different groups can be found in Table 1.

Table 1. Treatment groups used to optimize ultrasound parameters

Group	MI*	Flash†	No. of animals	Figure	Expected MB behavior‡
1			3		
2	0.1		3	2B	Limited destruction
3	0.1	3 cycles of MI1	3	2C	
4		3 cycles of MI1	3	2D	
5	0.25		2		Significant destruction
6	0.5		3	2E	Complete destruction
7	1		1§		Complete destruction

MI = mechanical index; MB = microbubble; PRF = pulse repetition frequency.

* Treatment was 10,000 cycles, local PRF = 10 Hz for 0.5-s treatment, followed by 1.5-s break and thus a global PRF 0.5 Hz, for a total of 2 min.

† To destroy the bubbles after oscillation, at a PRF of 0.5 Hz.

‡ As observed *in vitro* in a flow phantom.

§ Because tissue damage was observed with this treatment, only one animal was treated.

Blood vessels were stained by intra-venously injecting 100 μL fluorescein-labeled *Lycopersicon esculentum* (tomato) lectin (FITC-lectin, Sigma-Aldrich) diluted in 0.9% NaCl to 1 mg/mL (5 mg/kg) 2 h post-treatment, and allowing it to circulate for 5 min before euthanasia. The tumors were excised and sectioned for imaging by CLSM or for histologic evaluation as described below.

Confocal imaging of tumor sections and quantification of nanoparticle delivery

The excised tumors were embedded in OCT Tissue Tek (Sakura, Alphen aan den Rijn, Netherlands) and frozen in liquid N_2. The first 1000 μm was removed, before three frozen sections of 25 μm and one section of 4 μm were prepared from five depth levels in the tumor, with 300 μm between levels. The sections were mounted on objective glass slides, and the microdistribution of NPs was imaged by CLSM (TCS SP5, Leica). In sequential scans, a DPSS 561 laser was used to excite NR668-labeled NPs, and fluorescence was detected at 590–650 nm. An argon laser at 488 nm was used to excite FITC-labeled vasculature, and fluorescence was detected at 500–550 nm. An HCX PL APO CS 20 × 0.7 dry objective was used, and tile scans of entire tumor sections were captured using a frame size of 512 × 512 pixels (775 × 775 μm) and 400-Hz scan speed. An optical section of 5 μm was used (airy unit 2.8, pinhole 170 μm), and images through the section were captured every 2.5 μm to make z-stacks. The laser intensity and detector gain were kept the same for all sections, and were set to minimize noise and use the gray scale. When acquiring tile scans, the sections were imaged dry because mounting medium disturbed the distribution of the fluorescence during long acquisition times. For more detailed example images of NP distribution, a zoom factor of 3 was used, resulting in images of 258.33 μm. These sections were mounted with Vectashield (Vector Laboratories, Burlingame, CA, USA) to image FITC, and selected areas were imaged within minutes after mounting.

The tile scans were processed using ImageJ to quantify the tumor uptake of NPs. A maximum intensity projection of each z-stack was made. An ROI was drawn around each section. The image was thresholded using the inbuilt ImageJ Yen algorithm (determined to give the most suitable thresholding by visual inspection), and "analyze particles" was used to quantify the number of above-threshold pixels and their intensity. The results were displayed as number of pixels divided by the area of the respective tumor section.

Histology

Tumors for histologic evaluation were fixed for a minimum of 2 d in 4% neutral buffered formaldehyde. The samples were then embedded in paraffin, before

4-μm sections (Leica Tissue processor) were made from the middle of the tumor. They were stained with hematoxylin, erythrosin and saffron (HES), and imaged to evaluate tissue damage after the US treatment. This will stain cell nuclei *blue-purple*, cytoplasm and ECM *pink*, erythrocytes *red* and collagen fibers in connective tissues *yellow*. The sections were analyzed by an experienced senior pathologist, blinded to which tumor received which treatment.

Treatment of triple-negative breast cancer MDA-MB-231 xenografts with NPMB-encapsulated cabazitaxel

The tumors were allowed to grow for 3 wk until they had reached approximately 4 mm in the longest direction. The number of animals and control groups was, in compliance with the "3 Rs" (replacement, reduction, refinement) (Fenwick et al. 2009), kept low in this pilot study. Twelve animals were randomly distributed into three groups: (1) animals injected with saline, control group; (2) animals injected with NPMBs containing cabazitaxel; (3) animals injected with NPMBs containing cabazitaxel and tumors exposed to the previously described US treatment (MI = 0.5).

The mice were treated 2 wk in a row (days 21 and 29 after implantation of cells). On the day of treatment, animals were anesthetized and the tail vein was cannulated. An intra-venous bolus of 200 μL saline or NPMBs was given. The concentration of NP in the bubble solution was 10 mg/mL, resulting in a total dose of 2 mg NPs per animal and, thus, 10 mg/kg cabazitaxel. This dose was chosen based on the literature (Semiond et al. 2013; Vrignaud et al. 2013, 2014). The optimal US treatment from the optimization of various MIs was used (group 6 with an MI of 0.5 as described above) for the first treatment. Unfortunately, the transducer broke after the first treatment. To continue the experiment, the second treatment was done with another transducer (RK-100 system, aperture = 52 mm and focal distance 60 = mm, FUS Instruments, Toronto, ON, Canada). It had a frequency of 1.1 MHz, and because of its smaller focal diameter, the transducer was scanned to cover the tumor area. Sixteen spots (4 × 4) were scanned during 3.5 s. In each spot, a burst of 10,000 cycles was transmitted at an MI of 0.5. The total treatment time was increased from 2 to 3.5 min to achieve 60 sonications, to make the treatment as similar as possible to the first treatment with the Imasonic transducer. The lateral 3- and 6-dB beam widths were 1.3 and 1.6 mm, respectively, while in the axial direction, 4 cm has a pressure within the 3-dB limit.

After the treatment, the antidote was administered to terminate anesthesia, and the animals were placed in a recovery rack until the next morning to avoid hypothermia in the recovery period. The rack maintained a temperature of 28°C. The day after a treatment, the animals were given Diet gel boost (ClearH_2O, Westbrook, ME, USA) as a supplement to the dry food. The tumor growth was measured using calipers and the animals were weighed two times per week for 14 wk after the end of treatment. The criteria for humane endpoints at which animals were euthanized were tumor diameter of 15 mm or weight loss of 15%.

A third treatment was planned a week after the second treatment, but the first two animals that received the third treatment (NPMBs with cabazitaxel) died shortly after the injection. Therefore, the remaining animals were not treated a third time. One animal in the control group (saline) was euthanized because the tail became partly necrotic.

Statistical analysis

A two-tailed unpaired *t*-test was used to evaluate if the difference in NP uptake between groups 1 and 6 was statistically significant (Excel 2010, Microsoft, Redmond, WA, USA). A p value < 0.05 was considered to indicate statistical significance.

RESULTS

Characterization of nanoparticles and microbubbles

The NPs had diameters in the range 140–195 nm (z-average), a PDI below 0.2 and ζ potential in the range -1 to -2.5 mV. The determined loading efficiency of cabazitaxel was close to 100% with a drug payload of 10 wt%.

The self-assembled MBs had an average mean diameter of 2.6 ± 1.3 μm. The concentration of MBs was approximately 5×10^8 MBs/mL. From characterization of NPMBs in the flow tube, the MBs exhibited very limited destruction at MI 0.1, partial destruction at MI 0.25 and complete destruction at MI 0.5 and 1 (Supplementary Fig. S3, online only, available at http://dx.doi.org/10.1016/j.ultrasmedbio.2017.06.029).

In vivo *circulation half-life of nanoparticles*

The *in vivo* circulation half-life of the PEGylated PEBCA NPs was found to be 136 min. An exponential decay, $f(t) = 206160.9e^{-0.0051t}$ fitted the experimental data of fluorescence intensity in blood ($R^2 = 0.67$ and p values ≤ 0.0001) (Fig. 3).

In vivo *circulation of microbubbles*

The MBs stabilized by the self-assembled NPs were found to be suitable for *in vivo* contrast-enhanced US imaging and image-guided drug delivery. The contrast enhancement in a tumor imaged by US is illustrated in Figure 4b. From an ROI surrounding the tumor, the contrast was quantified (Fig. 4c). NPMBs could be detected for

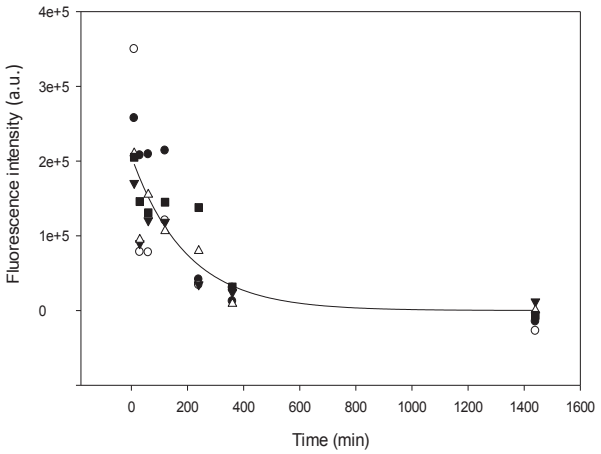

Fig. 3. Fluorescence intensity in blood as a function of time, and a mono-exponential decay $f(t) = 206{,}160.9e^{-0.0051t}$ fitted to the data. The various symbols represent different animals (n = 5).

approximately 4–5 min. NPMBs containing cabazitaxel were imaged in the kidney of a mouse, and inflow through the venous circulation could be seen before the MBs reached the arterial circulation and filled the kidney (Supplementary Fig. S4, online only, available at http://dx.doi.org/10.1016/j.ultrasmedbio.2017.06.029).

Biodistribution

The biodistribution of NPs was determined 6 h post-injection of NPMBs containing IR-780 lipid, when the NPs are nearly cleared from the circulation. Representative fluorescence intensities from organs and tumor from one animal are illustrated in Figure 5, as are the percentages of accumulated dose in the various tissues. A standard curve (Supplementary Fig. S1) was used to determine the amounts of NPs in the various tissues based on measured fluorescence intensities. The average weights of the respective organs, tumor and brain, are provided in Supplementary Table S1 (online only, available at http://dx.doi.org/10.1016/j.ultrasmedbio.2017.06.029). A total dose of 2 mg NPs (10 mg/mL × 0.2 mL) was injected into each animal, and about 1% of the dose was located in the tumor. The majority of the dose was located in the liver and spleen. Altogether, approximately 87% of the injected dose was found in spleen, liver, kidney, heart, lungs, tumor and brain. The rest is likely distributed in urine, stool, skin, muscle, bone, lymph nodes and other tissues.

Cellular uptake of nanoparticles

Cellular uptake of NPs in the breast cancer cell line was confirmed by CLSM (Fig. 6a). The NPs were imaged by detecting the encapsulated fluorescent dye NR668. FCM was used to quantify cellular uptake; 90% of the cells had taken up NPs by endocytosis after 3 h incubation (Fig. 6b), and the median fluorescence intensity was 18 times higher than the autofluorescence. No uptake was seen after incubation at 4°C, confirming that NR668 did not leak from the NPs, as previously reported (Snipstad et al. 2016; Sulheim et al. 2016).

In vitro *toxicity*

The *in vitro* toxicity of NPs with cabazitaxel for the breast cancer cell line MDA-MB-231 was determined with the AlamarBlue assay. Figure 7 indicates that the drug is effective against the cell line. The free drug is more effective than the encapsulated drug. After 24 h incubation, IC_{50} values were 5.7 and 1.1 for the encapsulated and free drug, respectively, whereas the y_{min} values were 37% and 32%. The ratio between the IC_{50} values was similar even at 72 h; however, the y_{min} values decreased with time (not shown). The empty NPs were by themselves not toxic, except for the highest concentration of 1000 ng/mL (not shown).

Microdistribution of nanoparticles

The microdistribution of NPs in the tumors 2 h post-US treatment was imaged using CLSM. Representative images from the control group that did not receive US treatment and a tumor treated with FUS at an MI of 0.5 are provided in Figure 8. Delivery of NPs to the treated tumor was increased compared with that to the control tumor. Many more NPs were seen in the FUS-treated tumor, and the NPs were displaced from the blood vessel into the ECM.

Quantification of nanoparticle tumor accumulation

To obtain a semiquantitative measurement of tumor uptake, CLSM tile scans of entire tumor sections from each animal were acquired and analyzed. One section from level 3 in each tumor was used (approximately 1.84 mm inside the tumor). A representative tile scan (Fig. 9a) depicts the variation in distribution of NPs across the tumor section (from group 6). The number of above-threshold pixels and their intensities were measured for each section. Results were displayed as the number of pixels divided by the area of the respective tumor section, for each animal in the different treatment groups (Fig. 9b). When presented as number of pixels multiplied by respective intensity, divided by area of the tumor section, the results were similar (not shown). Accumulation of NPs was not affected by low pressures (group 2 and 3), whereas the complete bubble destruction (group 6) and violent collapse of MBs at higher MIs (group 7) increased the delivery of NPs to tumors. The short flash at high MI (group 3 and 4) did not increase tumor uptake of NPs. To obtain more data points and information on the variation within tumors, sections from level 5 (approximately 2.6 mm inside the tumor) were also analyzed for groups 1 and 6 (Fig. 9c). In general, level 5

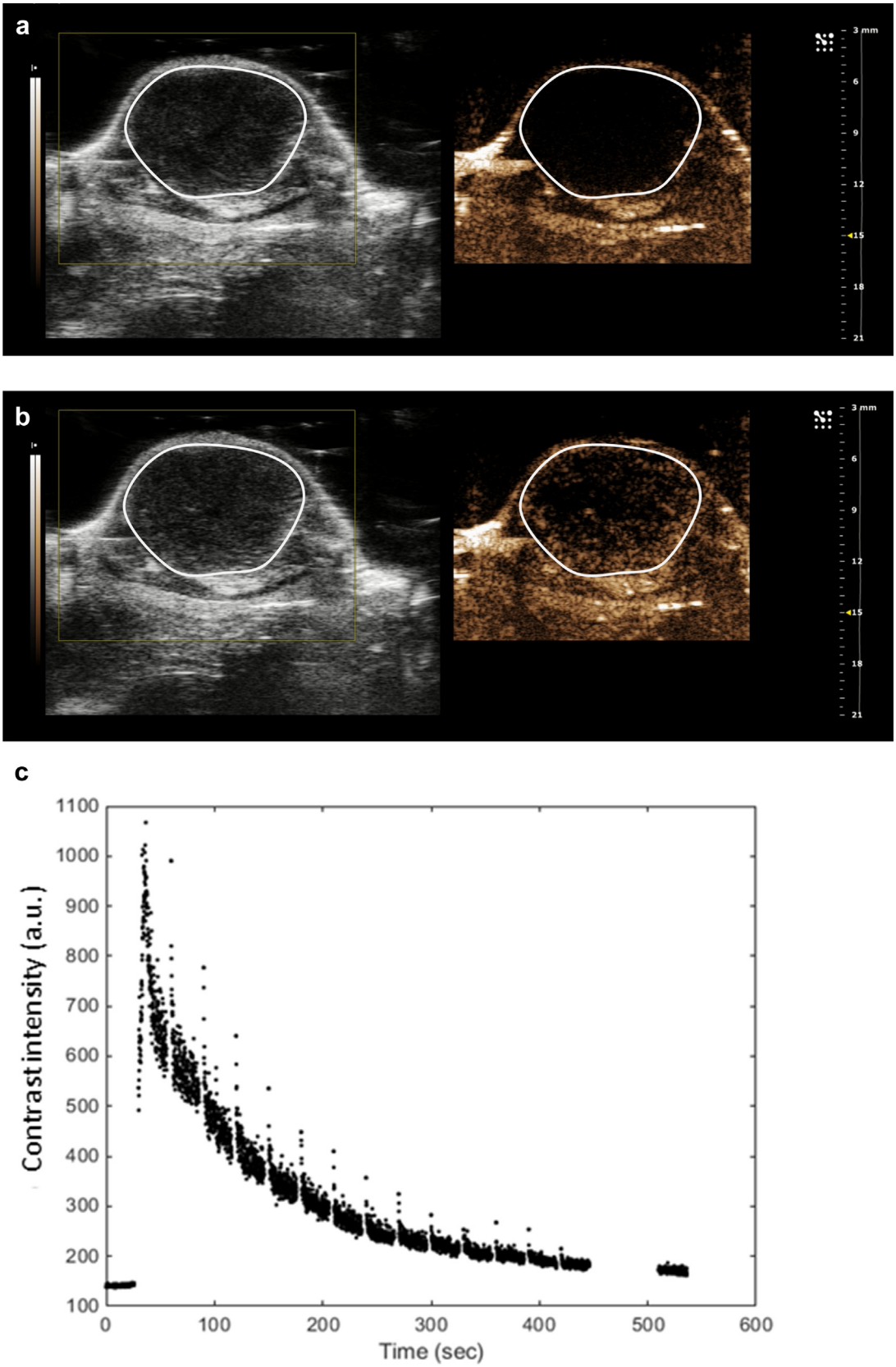

Fig. 4. Circulation of microbubbles. (a, b) Representative B-mode ultrasound (left) and non-linear contrast images (right) of a tumor pre-injection (a) and post-injection (b) of nanoparticle-stabilized microbubbles. (c) Contrast intensity was quantified (white region of interest), shown as a function of time to illustrate the time scale at which microbubbles are present in circulation.

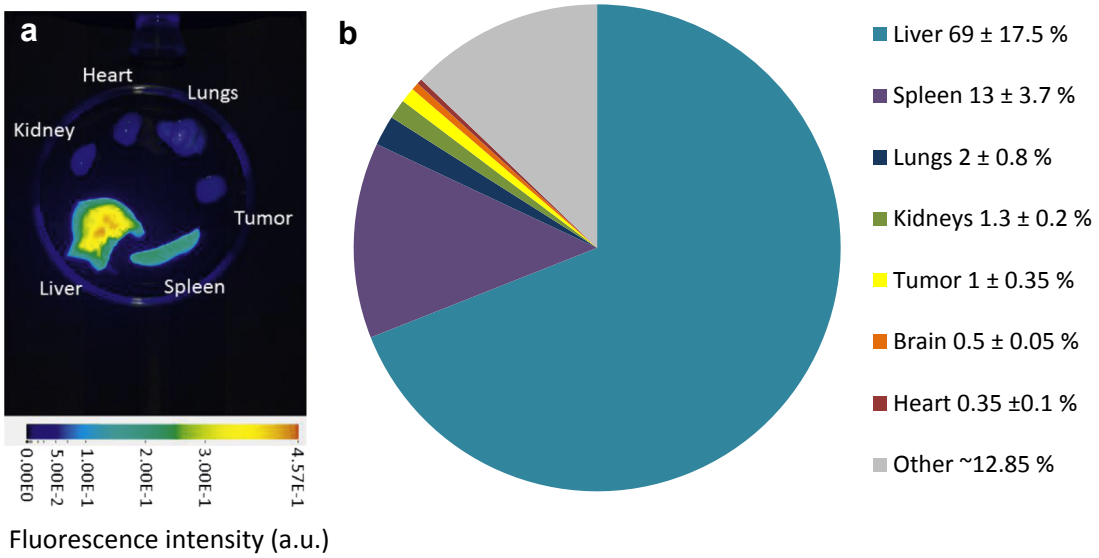

Fig. 5. Biodistribution of nanoparticles in the various organs, tumor and brain. (a) Representative fluorescence intensities from the various tissues. (b) Quantified percentage of nanoparticles in the various tissues. Means ± standard deviations of n = 4–7 animals.

sections exhibited lower NP uptake than level 3 sections. The overall mean relative fluorescence intensity in mice exposed to MI 0.5 was approximately 2.3 times higher than the mean of the control group that did not receive any US treatment, and the difference was statistically significant ($p = 0.0314$).

Histology

Except for the highest MI (group 7), which caused substantial visual hemorrhage, evaluation of HES-stained tumor sections revealed that all other FUS treatments could be considered tolerable. An example of an overview image of a non-treated tumor section and representative images of non-treated and treated tissue are provided in Figure 10. All sections, including the untreated, had some areas with a few microbleeds, but there were no significant differences between the different groups. The microbleeds could be from fragile neoangiogenic vessels, but there were no structural or histologic, morphologic or pathologic differences between the different treatment groups. The tumor was for the most circumscribed, with a necrotic core, and infiltrative growth in adjacent connective and muscular tissue was seen (Fig. 10a). Histologically, the tumor was highly cellular with varying degrees of atypia and a lot of mitotic cells. Thus, all characteristics of an aggressive, highly malignant tumor were present (Arpino et al. 2015; Zordoky et al. 2014). Observations of vasculature with malignant cells confirm a metastatic model.

Treatment of tumors with NPMBs containing cabazitaxel

As a proof-of-principle, to evaluate whether the increased delivery of NPs to the tumor tissue would be

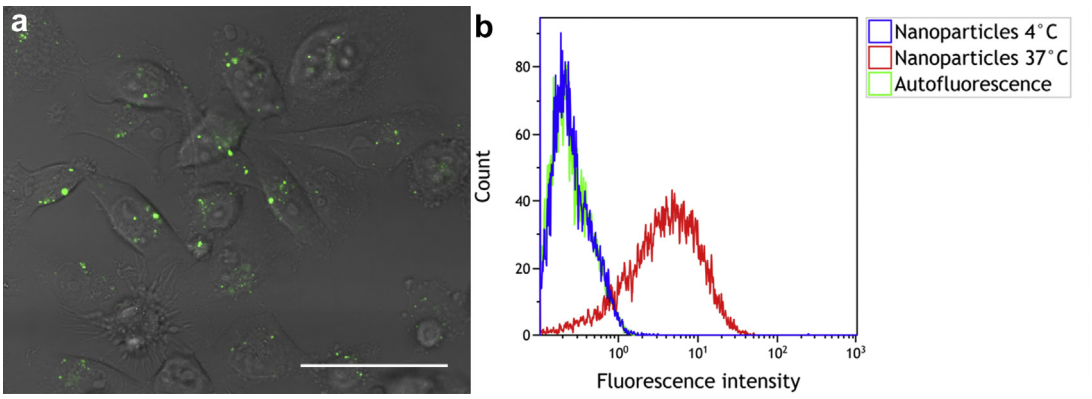

Fig. 6. Cellular uptake. (a) Confocal laser scanning microscopy and bright-field images of breast cancer MDA-MB-231 cells that have taken up nanoparticles. The encapsulated dye NR668 is shown in *green*. Bar = 50 μm. (b) Representative histogram from flow cytometry quantification of the uptake of nanoparticles after 3 h incubation at 4°C or 37°C.

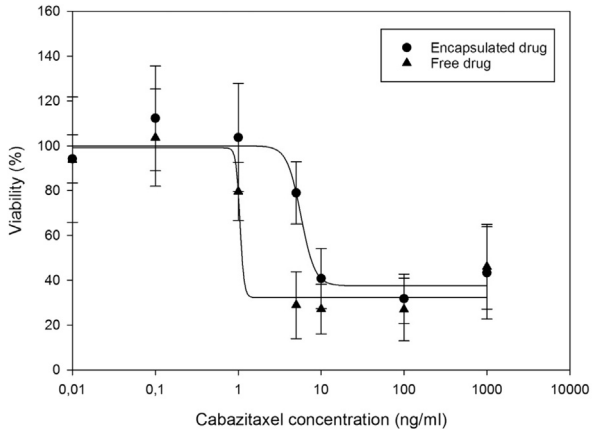

Fig. 7. Cytotoxicity of encapsulated and free cabazitaxel for the breast cancer cell line MDA-MB-231 after 24 h of exposure, measured with the AlamarBlue assay. The data are averages from n = 6 samples, with standard deviations. The percentage of viable cells is expressed as a function of drug concentration. Fitted dose–response curves are shown.

sufficient to improve treatment with encapsulated cytostatic drugs, a small treatment study was performed. The average tumor growth for the three treatment groups is illustrated in Figure 11. Untreated animals (saline) exhibited continuous tumor growth and were sacrificed on days 62, 69 and 72 after implantation when the tumors reached 15 mm. The group treated with NPMB-encapsulated cabazitaxel exhibited reduced tumor growth compared with the non-treated animals, and all animals responded to treatment, but with large variations in tumor volume between the animals. The tumors started regrowing approximately 80 d after implantation (50 d after treatment end). One animal was sacrificed on day 120 when the tumor reached 15 mm; the other two animals were still alive at the end of the study, with tumors of 13 and 4.5 mm in length. The group treated with FUS in addition to NPMBs with cabazitaxel had a larger reduction in tumor growth, and from day 48, all animals were in complete remission. At the end of the study, approximately 100 d after the end of treatment, all animals were still alive and in complete remission. Data points for all the individual animals are illustrated in Figure 11c–e, and indicate the variation in treatment response for the NPMB-treated tumors.

Neither the control animals nor the animals treated with encapsulated cabazitaxel and FUS lost any weight because of the treatment (Fig. 12).

DISCUSSION

In vivo *circulation and biodistribution*

In vivo circulation of NPs depends on particle material, shape, size, surface chemistry and charge and varies significantly between different NP formulations (Alexis et al. 2008; Longmire et al. 2008). For efficient delivery, the NPs must circulate for a sufficient time to accumulate in the target tissue, and avoid premature degradation and release of payload into the blood. Ideally, NPs that are not delivered to the target should be cleared before the particles release the drug. A common strategy to increase circulation is PEGylation, which prevents aggregation and creates a water corona around the NP. Generally, the water corona reduces protein adsorption and opsonization and, thus, prevents recognition by the reticuloendothelial system in liver and spleen (Harris and Chess 2003; Jokerst et al. 2011).

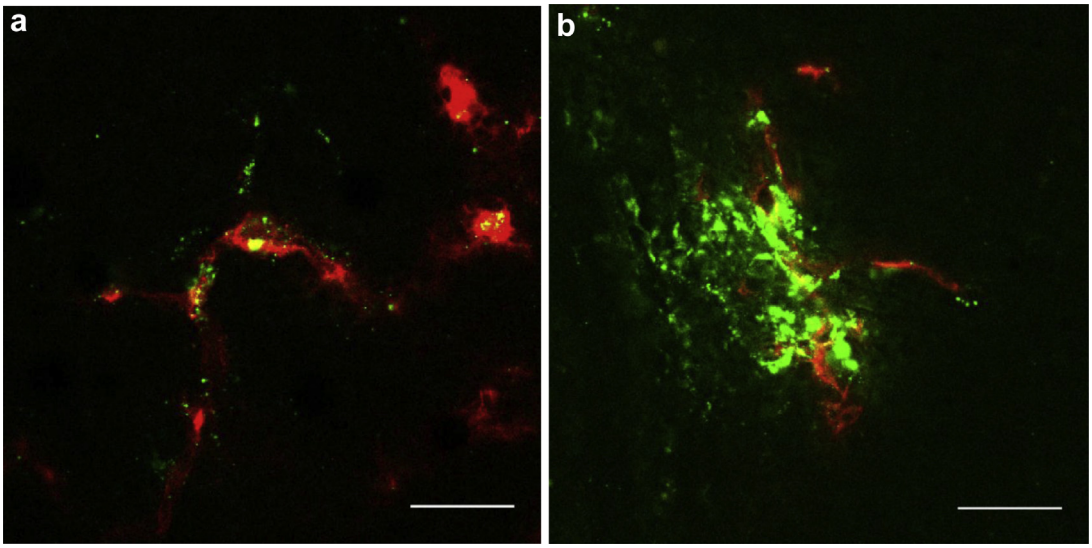

Fig. 8. Distribution of nanoparticles. Representative confocal laser scanning microscopy images from a tumor that did not receive any ultrasound treatment (a) and a tumor treated with a mechanical index of 0.5 (b). Blood vessels (fluorescein isothiocyanate) are in *red* and nanoparticles (NR668) in *green*. Bars = 50 μm.

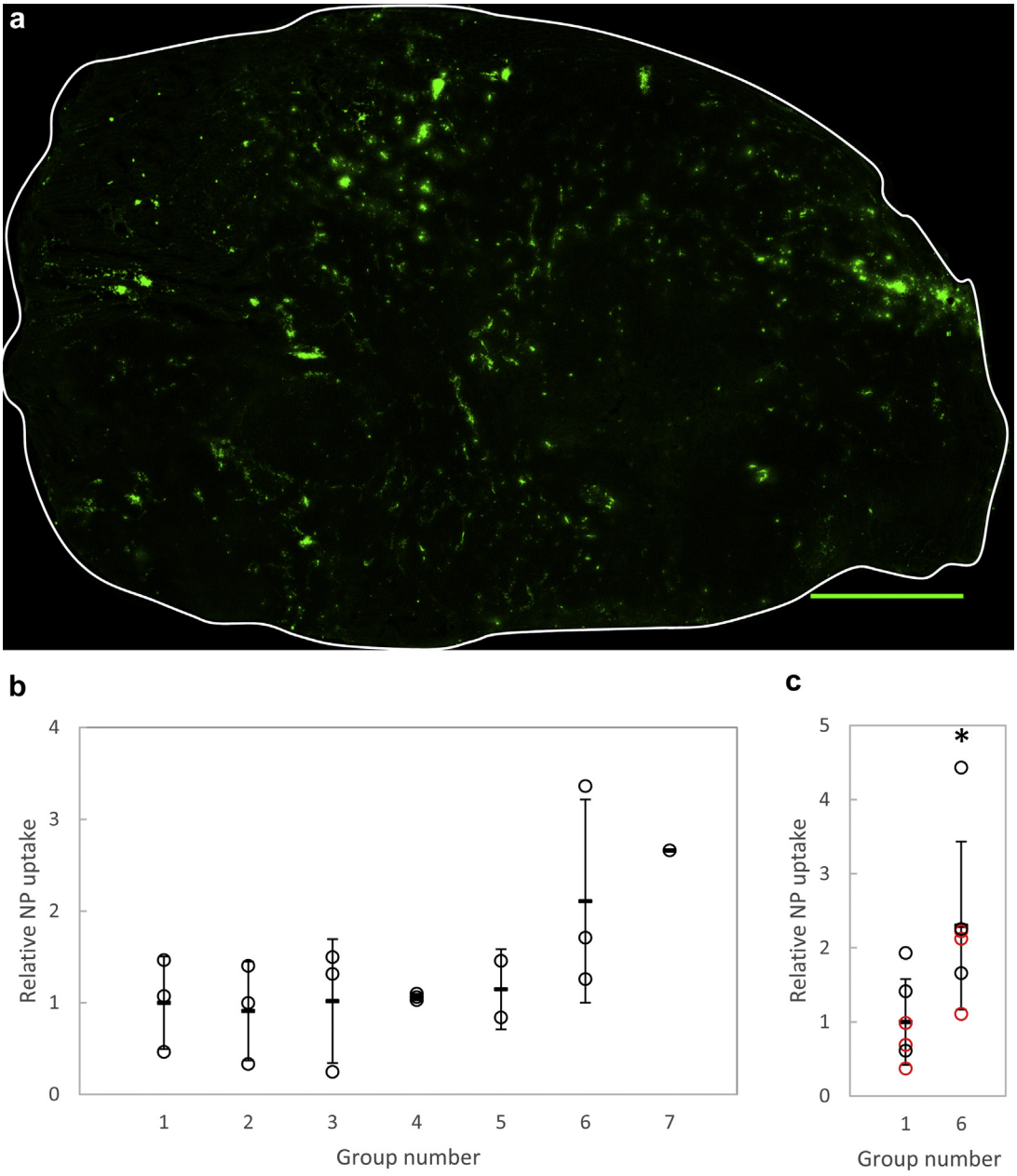

Fig. 9. Tumor uptake of nanoparticles. (a) Example of a confocal laser scanning microscopy tile scan from an entire tumor section from group 6 revealing nanoparticles (NPs) (NR668) in *green*. Bar = 1000 μm. The *white circle* represents the tumor border. (b) Quantification of number of pixels with NPs (NR668), divided by the area of the respective tumor section. Data points represent one level 3 section from each animal in the different treatment groups. Each individual animal is shown (○), together with the group mean (—) ± standard deviation. All data points are normalized to the mean of group 1. Group 1: control, no ultrasound (n = 3 animals). Group 2: mechanical index (MI) = 0.1, limited microbubble (MB) destruction (n = 3 animals). Group 3: MI = 0.1 + flash MI 1 (n = 3 animals). Group 4: flash MI 1 (n = 3 animals). Group 5: Significant MB destruction with intermediate MI of 0.25 (n = 2 animals). Group 6: Complete MB destruction with MI of 0.5 (n = 3 animals). Group 7: violent collapse MI 1 (n = 1 animal). Sections from both level 3 (*black*) and level 5 (*red*) are shown for groups 1 and 6 (c), n = 6 sections per group. The average in group 6 is 2.3 times higher than that in group 1; the difference between the two groups was statistically significant (*p = 0.0314).

The majority of opsonized particles are cleared within a few minutes because of the high concentrations of phagocytic cells in the liver and spleen, or they are excreted (Alexis et al. 2008). However, it has recently also been reported that PEG can affect the composition of the protein corona that forms around nanocarriers and

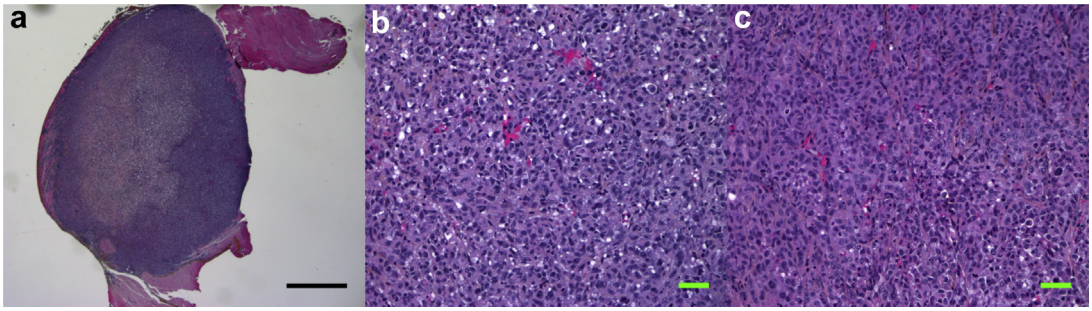

Fig. 10. Histology. Representative overview image of a hematoxylin, erythrosin and saffron stained section from an untreated breast cancer MDA-MB-231 tumor (a), and images of non-treated (b) and treated (c) tissue. Bars = 1000 μm (a) and 50 μm (b, c).

that the presence of distinct proteins is necessary to prevent non-specific cellular uptake (Schottler et al. 2016). The NPs used in the present work had a half-life of 136 min, which is more than three times that of their PBCA counterparts with similar PEGylation, as determined in our previous work (Åslund et al. 2017). The increased circulation is likely due to increased PEGylation, a decreased degradation rate (Muller et al. 1992; Sulheim et al. 2016) and presumably a slower dissociation/release of PEG from the particle surface. The more hydrophobic polymer (PEBCA vs. PBCA) could also provide stronger anchoring of the PEG, which is attached by hydrophobic interactions. Similar half-lives on the order of a few hours have also been reported by others, for PBCA NPs loaded with doxorubicin (Reddy and Murthy 2004) and for hexadecyl cyanoacrylate (PHDCA) NPs (Fang et al. 2006).

The amount of NPs accumulating in the tumor was measured when the NPs were nearly cleared from the circulation (6 h post-injection), and 1% of the injected NP dose was found to be located in the tumor. This corresponds well with the reported median of 0.7% from a survey of 117 reports during the past 10 y (Wilhelm et al. 2016), and with reported liposome uptake in human tumors (Harrington et al. 2001). This is a clear improvement compared with what has been reported for chemotherapeutic drugs, where only 0.001% to 0.01% of the injected drug reaches the tumor (Gerber et al. 2009; Kurdziel et al. 2011). The majority of the NPs were found in the liver and spleen, which corresponds well with the literature (Douglas et al. 1986; Harrington et al. 2001; Owens and Peppas 2006; Tang et al. 2014; Wilhelm et al. 2016), and would also be expected because these organs are responsible for clearing particles larger than 100 nm (Alexis et al. 2008; Desai 2012). As expected, fewer NPs were localized in the kidneys, likely because the NPs do not degrade much during this period (Sulheim et al. 2016).

The MBs were injected intra-venously, and could be imaged in venous and arterial circulation using a preclinical US scanner. In the tumor tissue, NPMBs could be detected for approximately 4–5 min, which is comparable to times for other commercial MBs (Hyvelin et al. 2013). The washout of MBs is due to MB collapse and clearance from the vasculature by reticuloendothelial system capture (Hyvelin et al. 2013). We cannot exclude that, in addition to circulating MBs, some MBs might be adhering to the microvasculature.

In vitro *cellular uptake and toxicity*

The uptake of PACA NPs has been observed to vary greatly between different cell lines and for NPs of different polymers (Sulheim et al. 2016). The efficient *in vitro* uptake of PEBCA NPs observed for the MDA-MB-231 breast cancer cell line indicates that once the NPs have reached the tumor interstitium, they can effectively be taken up by the breast cancer cells by endocytosis. Once the NPs have been internalized, they should eventually degrade to release the cytostatic cargo. Based on the *in vitro* toxicity, this cell line responds well to the drug, and the encapsulated drug is also efficient. If the NPs were not internalized, alternative mechanisms would be that the NPs degrade and release the drug extracellularly, followed by cellular uptake of the free drug, or that the drug is delivered by direct contact-mediated transfer into cells, which has been observed for other hydrophobic model drugs (Snipstad et al. 2014). The degradation of PACA nanoparticles has been characterized previously (Sulheim et al. 2016), and occurs mainly by surface erosion after hydrolysis of the ester bond of the alkyl side chain of the polymer, resulting in the degradation products alkyl alcohol and poly(cyanoacrylic acid), which are excreted by the kidneys (Vauthier et al. 2003).

Ultrasound-enhanced delivery of nanoparticles

To determine the optimal treatment for this NPMB and achieve enhanced delivery of NPs to the tumor tissue, various US treatments were investigated. An understanding of cavitation processes is crucial to maximizing efficiency and tolerability in US-mediated drug delivery. The response of a MB to US depends highly on the frequency,

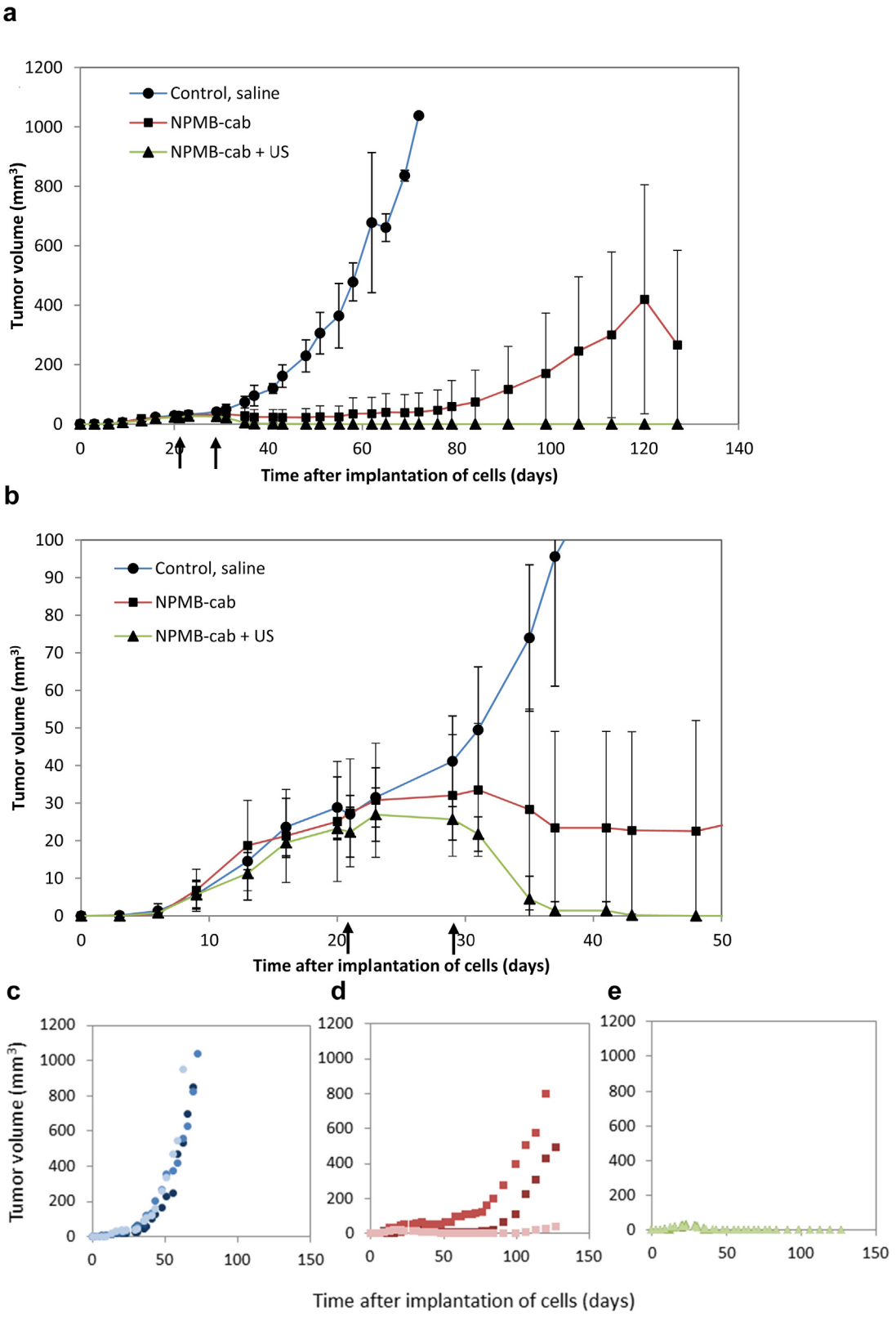

Fig. 11. Tumor volume as a function of time after implantation of cells (day 0). (a) Mice were treated with saline, nanoparticle-stabilized microbubbles (NPMBs) with cabazitaxel or NPMBs with cabazitaxel and focused ultrasound (a). Treatments were performed on days 21 and 29 (*arrows*). Data are means and standard deviations from n = 4 animals in each group until day 35 and from n = 3 animals per group from day 37. (b) Zoomed-in figure is shown for the first 50 d. (c–e) Data points for all the individual animals treated with saline (c), NPMBs with cabazitaxel (d) and NPMBs with cabazitaxel and focused ultrasound (e), with different colors representing different animals.

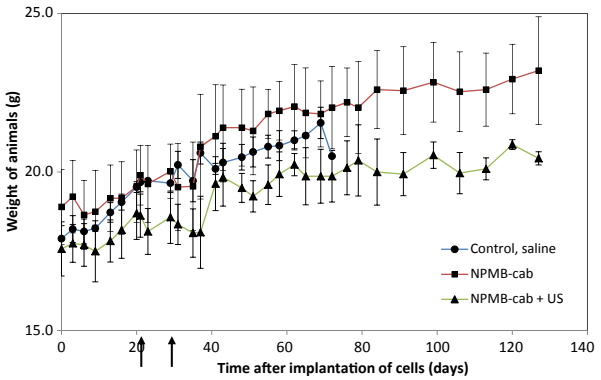

Fig. 12. Weight of treated animals after implantation of cells (day 0) and treatments with saline, nanoparticle-stabilized microbubbles (NPMBs) with cabazitaxel or NPMBs with cabazitaxel and focused ultrasound. Treatments were performed on days 21 and 29 (*arrows*). Data are means and standard deviations from n = 4 animals in each group until day 35 and from n = 3 animals from day 37.

pressure level and pulse duration (Lammertink et al. 2015; Lentacker et al. 2014), as well as properties of the MB such as size, shell thickness and stiffness (Lentacker et al. 2014). The effect of US-mediated delivery of NPs also depends on tumor characteristics as the barriers for delivery of nanomedicine can vary greatly between tumor types.

In the breast cancer model used here, lower acoustic pressures (MI of 0.1 or 0.25) did not enhance tumor uptake of NPs. Acoustic characterization (data not shown) and *in vitro* US contrast imaging of NPMBs have indicated that the NPMBs are acoustically active and oscillate at these pressure levels, and that there is partial destruction at an MI of 0.25. Still, these low pressures did not affect the vascular permeability enough to allow extravasation of NPs *in vivo*. It has been suggested that US intensities may be adapted to create pore sizes that correlate with drug size (Lentacker et al. 2014), and that delivery of larger agents such as NPs may require higher US pressures compared with delivery of low-molecular-weight drugs (Wang et al. 2015).

At higher acoustic pressures (MIs of 0.5 and 1), the delivery of NPs to tumors was improved, indicating that complete destruction of the NPMB is necessary for enhanced permeability. At an MI of 0.5, there was significantly improved tumor accumulation; the amount of NPs delivered was, on average, 2.3 times higher than that for the non-treated group. If the MB is located close enough to the capillary wall, the oscillating and collapsing MB will induce forces on the endothelial cells through shear stresses, fluid streaming, shock waves and jet streams. The increased extravasation and distribution of NPs are thus likely due to one or a combination of the following: increased vascular permeability through increased number of fenestrations, increased endocytosis/exocytosis of NPs in endothelial cells and increased fluid convection in the vasculature and interstitium (Burke et al. 2014; Frenkel 2008; Lentacker et al. 2014). The variation in NP accumulation within treatment groups is likely due to the different amounts of vasculature between different tumors, as well as variations in leakiness of the vasculature and different size of the necrotic core. The short flash of MI 1 did not improve the uptake of NPs, indicating that a longer pulse is needed. The longer pulse might push the MB toward the vessel wall, possibly resulting in closer proximity to the endothelial cells at the time of the MB bursts. During the long pulse, the NPMB will burst, and the released gas can form new and possibly smaller MBs, which again will oscillate and potentially coalesce. Altogether, long pulses facilitate sustained bio-effects from the oscillating bubbles.

Except for the highest MI (1.0), which caused substantial visual hemorrhage, evaluation of HES-stained tumor sections revealed that all other FUS treatments can be considered tolerable. When bleeding is induced by inertial cavitation, a large amount of extravasated NPs would also be expected. The fact that tissue damage was observed at MI 1, but not at 0.5, suggests that the threshold for inertial cavitation is > 0.5 for our NPMBs. This indicates a window where enhanced accumulation can be achieved without damaging the tissue, at an MI of 0.5.

Focused US-mediated delivery of NPs to tumor tissue has been reported by others using MIs even higher than those used here. High pressure (1 MHz, 1.2 MPa) was used by Lin et al. (2010) to deliver lipid-coated quantum dots by pulsed FUS and SonoVue, and they concluded that they effectively enhanced vascular permeability in the sonicated tumors. They reported no cellular damage in the sonicated tumors. They did, however, use a slightly lower duty cycle of 1%. The same treatment was used to increase delivery of PEGylated liposomal doxorubicin (Lin et al. 2012). Wang et al. (2015) hypothesized that delivery of nanocarriers similar in size to those used in our work required inertial cavitation. They used a subcutaneous, well-vascularized xenograft of human colon cancer in mice, and found that the amount of NPs delivered increased with increasing acoustic pressures. They reported that US induced only minimal tissue damage, but slightly increased hemorrhage was observed at higher acoustic pressures (1.8 MHz, 0–6.9 MPa). They used 1000 bursts of 5 cycles delivered at a PRF of 100 Hz.

The direct association between NPs and MBs will probably result in a higher local concentration of NPs when the MBs are destroyed, compared with co-injection of NPs and MBs. Burke et al. (2014) used poly(lactic-co-glycolic acid) (PLGA) NPs linked to MBs and found that ultrasonic activation of the MBs increased delivery to the tumor, and that the loaded drug 5-fluorouracil could

reduce tumor growth and prolong survival in mice with subcutaneous, well-vascularized C6 gliomas. Their NPs were similar in size to those used here, and Burke et al. reported that coupling the NPs to MBs resulted in more efficient delivery compared with a co-injection of NPs and MBs.

Treatment of tumors with NPMBs loaded with cabazitaxel

The efficient reduction in tumor growth observed using our NPMBs in combination with FUS is highly promising for enhanced, localized delivery of encapsulated chemotherapeutic drugs. The tumors treated with NPMBs with cabazitaxel and FUS went into complete remission. This is probably due to the enhanced accumulation and improved distribution of NPs, observed after FUS exposure of MI 0.5, and the effective cellular uptake.

All tumors treated with NPMB-encapsulated cabazitaxel, but no FUS, responded to treatment and exhibited reduced growth compared with control animals. They were in stable remission until approximately 80 d after implantation (50 d after treatment end), before starting to regrow with large variation between the animals. The improved therapeutic response combining FUS with NPMBs, compared with NPMBs alone, indicates that the EPR effect for the NPs was not sufficient on its own. This could be due to low vascular density and permeability, as well as necrotic regions. Cabazitaxel, like the other taxanes, binds to tubulin molecules and, thus, inhibits microtubule depolymerization, thereby blocking mitosis and causing cell death (McGrogan et al. 2008; Vrignaud et al. 2013, 2014). Cabazitaxel has been found to be effective against tumors with resistance to other taxanes, and it affects predominantly tissue with a high cell turnover. It is thus possible that some quiescent cells respond less, causing the observed variations between tumors. For the treatment to be curative, every single cell must be eradicated. However, cancer cells with therapeutic resistance, such as hypoxic cells and cancer stem cells, may reside in perinecrotic and/or hypoxic regions and niches with low accumulations of nanocarriers (Hansen et al. 2015).

With respect to the tolerability and toxicity of the treatment, weight loss, which is a common side effect of treatment with cytostatic drugs, was not observed for any of the treatments, nor was FUS-induced bleeding observed using an MI at 0.5.

Focused ultrasound treatment with MBs and nanomedicine could possibly be used as a curative treatment, as neoadjuvant chemotherapy for solid tumors followed by surgical resection or in combination with/after surgery or radiation to remove residual cells. The first clinical phase I trial combining FUS and MBs with chemotherapy has already been reported; 10 patients with inoperable, locally advanced pancreatic cancer received an infusion of gemcitabine, followed by SonoVue injected intra-venously during US treatment (Dimcevski et al. 2016). These results illustrate the potential of combining FUS with MBs for increased efficacy of therapeutic drugs, and indicates that our NPMB is a promising novel platform for such applications.

CONCLUSIONS

Ultrasound sonication and destruction of NPMBs were found to substantially improve the accumulation and distribution of NPs in tumors, at a tolerable pressure level. US in combination with NPMB-encapsulated cabazitaxel resulted in complete, stable remission in all treated animals, clearly indicating that this unique NPMB platform is very useful for controlled drug delivery.

Acknowledgments—Dr. Andrey Klymchenko is acknowledged for kindly providing NR668, and Kristin Sæterbø, Andreas Åslund, Anne Rein Hatletveit, Maria Gellein, Sven Even Borgos and Kai Vernstad, for technical support. Housing and care of animals were provided by the Comparative Medicine Core Facility (CoMed), and tissue sections were prepared by the Cellular and Molecular Imaging Core Facility (CMIC), both at NTNU. The project was funded by the Central Norway Regional Health Authorities (46070000) and the Research Council of Norway (240410/F20 Multibubble and 254832/O70 BubbleCAN).

SUPPLEMENTARY DATA

Supplementary data related to this article can be found online at http://dx.doi.org/10.1016/j.ultrasmedbio.2017.06.029.

REFERENCES

Afadzi M, Strand SP, Nilssen EA, Måsøy SE, Johansen TF, Hansen R, Angelsen BA, Davies CL. Mechanisms of the ultrasound-mediated intracellular delivery of liposomes and dextrans. IEEE Trans Ultrason Ferroelectr Freq Control 2013;60:21–33.

Alexis F, Pridgen E, Molnar LK, Farokhzad OC. Factors affecting the clearance and biodistribution of polymeric nanoparticles. Mol Pharm 2008;5:505–515.

Anchordoquy TJ, Barenholz Y, Boraschi D, Chorny M, Decuzzi P, Dobrovolskaia MA, Farhangrazi ZS, Farrell D, Gabizon A, Ghandehari H, Godin B, La-Beck NM, Ljubimova J, Moghimi SM, Pagliaro L, Park JH, Peer D, Ruoslahti E, Serkova NJ, Simberg D. Mechanisms and barriers in cancer nanomedicine: Addressing challenges, looking for solutions. ACS Nano 2017;11:12–18.

Arpino G, Milano M, De Placido S. Features of aggressive breast cancer. Breast 2015;24:594–600.

Åslund AKO, Berg S, Hak S, Mørch Ý, Torp SH, Sandvig A, Widerøe M, Hansen R, Davies CL. Nanoparticle delivery to the brain—By focused ultrasound and self-assembled nanoparticle-stabilized microbubbles. J Control Release 2015;220:287–294.

Åslund AKO, Sulheim E, Snipstad S, von Haartman E, Baghirov H, Starr NJ, Kvåle Løvmo M, Lelu S, Scurr DJ, Davies CL, Schmid RB, Mørch ÝA. Quantification and qualitative effects of different PEGylations on poly(butyl cyanoacrylate). Mol Pharm 2017; http://dx.doi.org/10.1021/acs.molpharmaceut.6b01085 [Epub ahead of print].

Baghirov H, Melikishvili S, Mørch Ý, Sulheim E, Åslund AKO, Hianik T, Davies CL. The effect of poly(ethylene glycol) coating and monomer type on poly(alkyl cyanoacrylate) nanoparticle interactions with lipid monolayers and cells. Colloids Surf B Biointerfaces 2017;150:373–383.

Burgess A, Ayala-Grosso CA, Ganguly M, Jordao JF, Aubert I, Hynynen K. Targeted delivery of neural stem cells to the brain using MRI-guided focused ultrasound to disrupt the blood–brain barrier. PLoS One 2011;6:e27877.

Burke CW, Alexander ET, Timbie K, Kilbanov AL, Price RJ. Ultrasound-activated agents comprised of 5FU-bearing nanoparticles bonded to microbubbles inhibit solid tumor growth and improve survival. Mol Ther 2014;22:321–328.

Carpentier A, Canney M, Vignot A, Reina V, Beccaria K, Horodyckid C, Karachi C, Leclercq D, Lafon C, Chapelon JY, Capelle L, Cornu P, Sanson M, Hoang-Xuan K, Delattre JY, Idbaih A. Clinical trial of blood–brain barrier disruption by pulsed ultrasound. Sci Transl Med 2016;8:343re2.

Chauhan VP, Stylianopoulos T, Boucher Y, Jain RK. Delivery of molecular and nanoscale medicine to tumors: Transport barriers and strategies. Annu Rev Chem Biomol Eng 2011;2:281–298.

Desai N. Challenges in development of nanoparticle-based therapeutics. AAPS J 2012;14:282–295.

Dimcevski G, Kotopoulis S, Bjånes T, Hoem D, Schjøtt J, Gjertsen BT, Biermann M, Molven A, Sorbye H, McCormack E, Postema M, Gilja OH. A human clinical trial using ultrasound and microbubbles to enhance gemcitabine treatment of inoperable pancreatic cancer. J Control Release 2016;243:172–181.

Douglas SJ, Davis SS, Illum L. Biodistribution of poly(butyl 2-cyanoacrylate) nanoparticles in rabbits. Int J Pharm 1986;34:145–152.

Downs ME, Buch A, Karakatsani ME, Konofagou EE, Ferrera VP. Blood–brain barrier opening in behaving non-human primates via focused ultrasound with systemically administered microbubbles. Sci Rep 2015;5:15076.

Eggen S, Fagerland SM, Mørch Ý, Hansen R, Søvik K, Berg S, Furu H, Bohn AD, Lilledahl MB, Angelsen A, Angelsen B, Davies CL. Ultrasound-enhanced drug delivery in prostate cancer xenografts by nanoparticles stabilizing microbubbles. J Control Release 2014;187:39–49.

Elder SA. Cavitation microstreaming. J Acoust Soc Am 1959;31:54–64.

Etheridge ML, Campbell SA, Erdman AG, Haynes CL, Wolf SM, McCullough J. The big picture on nanomedicine: The state of investigational and approved nanomedicine products. Nanomedicine (Lond) 2013;9:1–14.

Fang C, Shi B, Pei YY, Hong MH, Wu J, Chen HZ. In vivo tumor targeting of tumor necrosis factor-alpha-loaded stealth nanoparticles: Effect of MePEG molecular weight and particle size. Eur J Pharm Sci 2006;27:27–36.

Fenwick N, Griffin G, Gauthier C. The welfare of animals used in science: How the "Three Rs" ethic guides improvements. Can Vet J 2009;50:523–530.

Frenkel V. Ultrasound mediated delivery of drugs and genes to solid tumors. Adv Drug Deliv Rev 2008;60:1193–1208.

Gerber HP, Senter PD, Grewal IS. Antibody drug-conjugates targeting the tumor vasculature: Current and future developments. MAbs 2009;1:247–253.

Graham SM, Carlisle R, Choi JJ, Stevenson M, Shah AR, Myers RS, Fisher K, Peregrino MB, Seymour L, Coussios CC. Inertial cavitation to non-invasively trigger and monitor intratumoral release of drug from intravenously delivered liposomes. J Control Release 2014;178:101–107.

Hanahan D, Weinberg RA. Hallmarks of cancer: The next generation. Cell 2011;144:646–674.

Hansen AE, Petersen AL, Henriksen JR, Boerresen B, Rasmussen P, Elema DR, Rosenschold PM, Kristensen AT, Kjaer A, Andresen TL. Positron emission tomography based elucidation of the enhanced permeability and retention effect in dogs with cancer using copper-64 liposomes. ACS Nano 2015;9:6985–6995.

Harrington KJ, Mohammadtaghi S, Uster PS, Glass D, Peters AM, Vile RG, Stewart JS. Effective targeting of solid tumors in patients with locally advanced cancers by radiolabeled pegylated liposomes. Clin Cancer Res 2001;7:243–254.

Harris JM, Chess RB. Effect of pegylation on pharmaceuticals. Nat Rev Drug Discov 2003;2:214–221.

He C, Chan C, Weichselbaum RR, Fleming GF, Yamada SD, Lin W. Nanomedicine for combination therapy of cancer. EBioMedicine 2015;2:366–367.

Heath CH, Sorace A, Knowles J, Rosenthal E, Hoyt K. Microbubble therapy enhances anti-tumor properties of cisplatin and cetuximab in vitro and in vivo. Otolaryngol Head Neck 2012;146:938–945.

Hynynen K, McDannold N, Vykhodtseva N, Jolesz FA. Noninvasive MR imaging-guided focal opening of the blood–brain barrier in rabbits. Radiology 2001;220:640–646.

Hyvelin JM, Tardy I, Arbogast C, Costa M, Emmel P, Helbert A, Theraulaz M, Nunn AD, Tranquart F. Use of ultrasound contrast agent microbubbles in preclinical research recommendations for small animal imaging. Invest Radiol 2013;48:570–583.

Jokerst JV, Lobovkina T, Zare RN, Gambhir SS. Nanoparticle PEGylation for imaging and therapy. Nanomedicine (Lond) 2011;6:715–728.

Klymchenko AS, Roger E, Anton N, Anton H, Shulov I, Vermot J, Mely Y, Vandamme TF. Highly lipophilic fluorescent dyes in nano-emulsions: Towards bright non-leaking nano-droplets. RSC Adv 2012;2:11876–11886.

Kotopoulis S, Delalande A, Popa M, Mamaeva V, Dimcevski G, Gilja OH, Postema M, Gjertsen BT, McCormack E. Sonoporation-enhanced chemotherapy significantly reduces primary tumour burden in an orthotopic pancreatic cancer xenograft. Mol Imaging Biol 2014;16:53–62.

Kurdziel KA, Kalen JD, Hirsch JI, Wilson JD, Bear HD, Logan J, McCumisky J, Moorman-Sykes K, Adler S, Choyke PL. Human dosimetry and preliminary tumor distribution of F-18-fluoropaclitaxel in healthy volunteers and newly diagnosed breast cancer Patients Using PET/CT. J Nucl Med 2011;52:1339–1345.

Lammers T, Kiessling F, Hennink WE, Storm G. Nanotheranostics and image-guided drug delivery: Current concepts and future directions. Mol Pharm 2010;7:1899–1912.

Lammertink BH, Bos C, Deckers R, Storm G, Moonen CT, Escoffre JM. Sonochemotherapy: From bench to bedside. Front Pharmacol 2015;6:138.

Lentacker I, De Cock I, Deckers R, De Smedt SC, Moonen CT. Understanding ultrasound induced sonoporation: Definitions and underlying mechanisms. Adv Drug Deliv Rev 2014;72:49–64.

Lin CY, Huang YL, Li JR, Chang FH, Lin WL. Effects of focused ultrasound and microbubbles on the vascular permeability of nanoparticles delivered into mouse tumors. Ultrasound Med Biol 2010;36:1460–1469.

Lin CY, Li JR, Tseng HC, Wu MF, Lin WL. Enhancement of focused ultrasound with microbubbles on the treatments of anticancer nanodrug in mouse tumors. Nanomedicine (Lond) 2012;8:900–907.

Longmire M, Choyke PL, Kobayashi H. Clearance properties of nano-sized particles and molecules as imaging agents: Considerations and caveats. Nanomedicine (Lond) 2008;3:703–717.

Maeda H. Toward a full understanding of the EPR effect in primary and metastatic tumors as well as issues related to its heterogeneity. Adv Drug Deliv Rev 2015;91:3–6.

Maeda H, Wu J, Sawa T, Matsumura Y, Hori K. Tumor vascular permeability and the EPR effect in macromolecular therapeutics: A review. J Control Release 2000;65:271–284.

Marquet F, Tung YS, Teichert T, Ferrera VP, Konofagou EE. Noninvasive, transient and selective blood–brain barrier opening in non-human primates in vivo. PloS One 2011;6:e22598.

McGrogan BT, Gilmartin B, Camey DN, McCann A. Taxanes, microtubules and chemoresistant breast cancer. Biochim Biophys Acta 2008;1785:96–132.

Meijering BD, Juffermans LJ, van Wamel A, Henning RH, Zuhorn IS, Emmer M, Versteilen AM, Paulus WJ, van Gilst WH, Kooiman K, de Jong N, Musters RJ, Deelman LE, Kamp O. Ultrasound and microbubble-targeted delivery of macromolecules is regulated by induction of endocytosis and pore formation. Circ Res 2009;104:679–687.

Mørch Ý, Hansen R, Berg S, Åslund AKO, Glomm WR, Eggen S, Schmid RB, Johnsen H, Kubowicz S, Snipstad S, Sulheim E, Hak S, Singh G, McDonagh BH, Blom H, Davies CL, Stenstad PM. Nanoparticle-stabilized microbubbles for multimodal imaging and drug delivery. Contrast Media Mol Imaging 2015;10:356–366.

Muller RH, Lherm C, Herbort J, Blunk T, Couvreur P. Alkylcyanoacrylate drug carriers: 1. Physicochemical characterization of nanoparticles with different alkyl chain-length. Int J Pharm 1992;84:1–11.

Nicolas J, Couvreur P. Synthesis of poly(alkyl cyanoacrylate)-based colloidal nanomedicines. Wiley Interdiscip Rev Nanomed Nanobiotechnol 2009;1:111–127.

Owens DE, Peppas NA. Opsonization, biodistribution, and pharmacokinetics of polymeric nanoparticles. Int J Pharm 2006;307: 93–102.

Padera TP, Stoll BR, Tooredman JB, Capen D, di Tomaso E, Jain RK. Pathology: Cancer cells compress intratumour vessels. Nature 2004;427:695.

Pitt WG, Husseini GA, Staples BJ. Ultrasonic drug delivery—A general review. Expert Opin Drug Deliv 2004;1:37–56.

Prabhakar U, Maeda H, Jain RK, Sevick-Muraca EM, Zamboni W, Farokhzad OC, Barry ST, Gabizon A, Grodzinski P, Blakey DC. Challenges and key considerations of the enhanced permeability and retention effect for nanomedicine drug delivery in oncology. Cancer Res 2013;73:2412–2417.

Reddy LH, Murthy RS. Pharmacokinetics and biodistribution studies of doxorubicin loaded poly(butyl cyanoacrylate) nanoparticles synthesized by two different techniques. Biomed Pap Med Fac Univ Palacky Olomouc Czech Repub 2004;148:161–166.

Schottler S, Becker G, Winzen S, Steinbach T, Mohr K, Landfester K, Mailander V, Wurm FR. Protein adsorption is required for stealth effect of poly(ethylene glycol)- and poly(phosphoester)-coated nanocarriers. Nat Nanotechnol 2016;11:372–377.

Semiond D, Sidhu SS, Bissery MC, Vrignaud P. Can taxanes provide benefit in patients with CNS tumors and in pediatric patients with tumors? An update on the preclinical development of cabazitaxel. Cancer Chemother Pharmacol 2013;72:515–528.

Snipstad S, Westrøm S, Mørch Ý, Afadzi M, Åslund AKO, Davies CL. Contact-mediated intracellular delivery of hydrophobic drugs from polymeric nanoparticles. Cancer Nanotechnol 2014;5:8.

Snipstad S, Hak S, Baghirov H, Sulheim E, Mørch Ý, Lélu S, von Haartman E, Bäck M, Nilsson KPR, Klymchenko AS, Davies CL, Åslund AKO. Labeling nanoparticles: Dye leakage and altered cellular uptake. Cytometry A 2016; http://dx.doi.org/10.1002/cyto.a.22853 [Epub ahead of print].

Soma E, Attali P, Merle P. A clinically relevant case study: The development of Livatag® for the treatment of advanced hepatocellular carcinoma. In: Alonso MJ, Csaba NJ, (eds). Nanostructured biomaterials for overcoming biological barriers. RSC Drug Discovery Series No. 22, Royal Society of Chemistry; 2012. p. 591–600.

Sulheim E, Baghirov H, von Haartman E, Bøe A, Åslund AKO, Mørch Ý, Davies CL. Cellular uptake and intracellular degradation of poly(alkyl cyanoacrylate) nanoparticles. J Nanobiotechnol 2016; 14:1.

Tang L, Yang XJ, Yin Q, Cai KM, Wang H, Chaudhury I, Yao C, Zhou Q, Kwon M, Hartman JA, Dobrucki IT, Dobrucki LW, Borst LB, Lezmig S, Helferich WG, Ferguson AL, Fan TM, Cheng JJ. Investigating the optimal size of anticancer nanomedicine. Proc Natl Acad Sci USA 2014;111:15344–15349.

Taurin S, Nehoff H, Greish K. Anticancer nanomedicine and tumor vascular permeability; Where is the missing link? J Control Release 2012;164:265–275.

van Wamel A, Sontum PC, Healey A, Kvåle S, Bush N, Bamber J, Davies CL. Acoustic cluster therapy (ACT) enhances the therapeutic efficacy of paclitaxel and Abraxane for treatment of human prostate adenocarcinoma in mice. J Control Release 2016;236:15–21.

Vauthier C, Dubernet C, Fattal E, Pinto-Alphandary H, Couvreur P. Poly(alkylcyanoacrylates) as biodegradable materials for biomedical applications. Adv Drug Deliv Rev 2003;55:519–548.

Vauthier C, Labarre D, Ponchel G. Design aspects of poly(alkylcyanoacrylate) nanoparticles for drug delivery. J Drug Target 2007;15: 641–663.

Vrignaud P, Semiond D, Lejeune P, Bouchard H, Calvet L, Combeau C, Riou JF, Commercon A, Lavelle F, Bissery MC. Preclinical antitumor activity of cabazitaxel, a semisynthetic taxane active in taxane-resistant tumors. Clin Cancer Res 2013;19:2973–2983.

Vrignaud P, Semiond D, Benning V, Beys E, Bouchard H, Gupta S. Preclinical profile of cabazitaxel. Drug Des Dev Ther 2014;8:1851–1867.

Wang TY, Choe JW, Pu KY, Devulapally R, Bachawal S, Machtaler S, Chowdhury SM, Luong R, Tian L, Khuri-Yakub B, Rao JH, Paulmurugan R, Willmann JK. Ultrasound-guided delivery of microRNA loaded nanoparticles into cancer. J Control Release 2015; 203:99–108.

Wilhelm S, Tavares AJ, Dai Q, Seiichi O, Audet J, Dvorak HF, Chan WCW. Analysis of nanoparticle delivery to tumours. Nat Rev Mater 2016;1:1–12.

Zordoky BN, Bark D, Soltys CL, Sung MM, Dyck JR. The anti-proliferative effect of metformin in triple-negative MDA-MB-231 breast cancer cells is highly dependent on glucose concentration: Implications for cancer therapy and prevention. Biochim Biophys Acta 2014;1840:1943–1957.